Journal of Computational and Applied Mathematics 229 (2009) 373–381

Contents lists available at ScienceDirect

Journal of Computational and Applied Mathematics

journal homepage: www.elsevier.com/locate/cam

A fractional differential equation for a MEMS viscometer used in the oil industry

A.D. Fitt [a,*], A.R.H. Goodwin [b], K.A. Ronaldson [a], W.A. Wakeham [c]

[a] *School of Mathematics, University of Southampton, Southampton SO17 1BJ, UK*

[b] *Schlumberger, 125 Industrial Blvd., Sugar Land, TX 77478, USA*

[c] *School of Engineering Sciences, University of Southampton, Southampton SO17 1BJ, UK*

ARTICLE INFO

Article history:
Received 19 May 2007
Received in revised form 26 September 2007

Keywords:
Fractional differential equation
Viscometer
Densimeter
MEMS device

ABSTRACT

A mathematical model is developed for a micro-electro-mechanical system (MEMS) instrument that has been designed primarily to measure the viscosity of fluids that are encountered during oil well exploration. It is shown that, in one mode of operation, the displacement of the device satisfies a fractional differential equation (FDE). The theory of FDEs is used to solve the governing equation in closed form and numerical solutions are also determined using a simple but efficient central difference scheme. It is shown how knowledge of the exact and numerical solutions enables the design of the device to be optimised. It is also shown that the numerical scheme may be extended to encompass the case of a nonlinear spring, where the resulting FDE is nonlinear.

1. Introduction

In this paper we analyse a device that has been designed to measure the viscosity of fluids that are encountered "downhole" during the process of oil well logging showing that, in one mode of operation, its motion is governed by a fractional differential equation. The oil exploration business places a high premium on optimum production strategies and the exploitation of downhole fluids such as crude oil or brine. When a test bore is drilled, a key indicator of whether or not the strata may contain oil involves the viscosity of the fluids that are encountered in the drill hole. *In situ* measurements of the thermophysical properties of these fluids are required and these may give crucial information concerning (for example) the permeability of the reservoir formation and its possible commercial value and flow characteristics.

1.1. Measurement of fluid thermophysical properties

The device that will be analysed below is a novel form of transversely oscillating micro-electro-mechanical system (MEMS) instrument. A device that can be deployed downhole possesses a number of important advantages. At present, it is normal for reservoir fluid samples to be collected, transported to the surface, and later analyzed in a surface laboratory. This *modus operandi* is not ideal, however, as the fluid's properties may change during its subsequent journey to the laboratory. This renders it difficult to faithfully simulate real reservoir conditions. A typical hydrocarbon reservoir is a hostile environment: pressures may range from 5 to 200 MPa and temperatures from 20 to 200 °C. Though it is not impossible to recreate such conditions in a laboratory, other downhole effects such as solid deposition and fluid contamination can be very

* Corresponding author.
E-mail addresses: adf@maths.soton.ac.uk (A.D. Fitt), Agoodwin@slb.com (A.R.H. Goodwin), kar@maths.soton.ac.uk (K.A. Ronaldson), vice-chancellor@soton.ac.uk (W.A. Wakeham).

0377-0427/$ – see front matter © 2008 Elsevier B.V. All rights reserved.
doi:10.1016/j.cam.2008.04.018

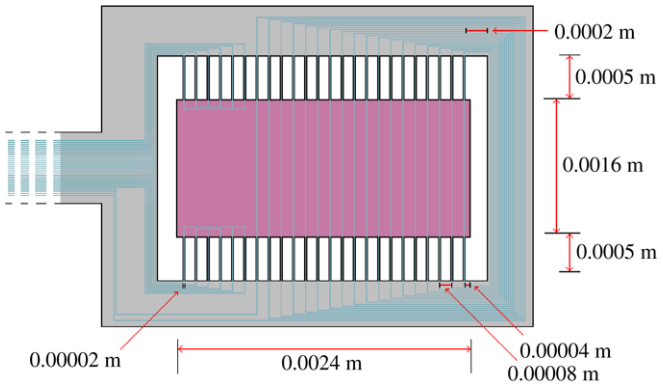

Fig. 1. Schematic and dimensions of the MEMS "spider" viscometry device.

much harder to simulate. Since reservoir fluid properties are frequently measured at ambient conditions, extrapolation is required to mimic reservoir conditions. Accurate rheological models are therefore needed, and the validity and applicability of the necessary theory may be hard to verify.

The advantages of a downhole measurement capability are thus clear. Though many different kinds of conventional viscometer have been developed and tested for laboratory use, most traditional viscometer designs are, for a variety of reasons, unsuitable for downhole deployment. Some contain moving parts that are separated by small clearances. Viscometers of this type are not only liable to become blocked by the solids (such as sand) that are frequently encountered during drilling, but also frequently suffer from the operational limitation that they must maintain a constant orientation with respect to the gravitational field. Torsional viscometers can perform poorly at high pressures owing to physical distortion and capillary devices are normally too involved and complicated to be deployed downhole. Disc viscometers are limited in their use as the fluids encountered in drilling applications are typically too viscous to allow such devices to perform accurately.

Until now, the only kind of device that has shown real promise for downhole deployment has been the simple and compact vibrating wire viscometer, for both its design and dimensions are well suited to the typically hostile environment that is encountered in oil exploration. If the velocity of the wire is estimated for several resonance frequencies and a range of currents, it is plausible that vibrating wire viscometers may yet provide useful measurements for both Newtonian and non-Newtonian fluids. However, the case for this kind of viscometer has yet to be proven with measurements.

1.2. A MEMS viscometer: The "spider"

The MEMS device, whose study is the purpose of this paper, is ideal for downhole deployment for a variety of reasons. It contains only a single moving part (all others being electrical), does not rely on being mounted in any specific orientation, can be mass-produced at low cost, and is extremely small and can therefore be mounted in very confined spaces. The device can also operate at high ambient pressures. Finally, as we shall see, the behaviour of the device may be analysed in a manner that allows its design to be optimised.

Full details of the composition, manufacture and further properties of the MEMS viscometer are given in [8]. In brief, the sensor, which is shown in Fig. 1 is composed primarily of pure silicon. Its large number of legs give rise to its informal name: the "spider". The MEMS fabrication technique used for the device is largely identical to that described in [2,3] for an edge-clamped plate that has been used to determine the density and viscosity of Newtonian fluids. As can be seen from the measurements in Fig. 1, the device, which contains both electrical and mechanical components, is extremely small. The oscillating plate is set into motion in its own plane when an alternating current I is passed through the wire coil on top of the plate, which is held in an externally-applied magnetic field. Motion detection in the device is provided by polysilicon piezoresistive strain gauges that are placed where maximum and minimum strains occur and form a Wheatstone bridge; the optimal positioning of the strain gauges is found by a finite element analysis. The device has 24 legs on each side. For the purposes of this study, it is simplest to assume that the "spider" can be forced to oscillate in any desired manner, though as we shall later see, this is not quite the case in reality.

The device may be used in two distinct fashions, which we shall term "forced" and "plucked" mode. In forced mode, the device is constrained to operate in a steady manner at a given frequency and various parameters of the motion are measured, from which the viscosity and/or density of the surrounding fluid may be inferred. In plucked mode, the device is released from an initial displacement and its subsequent decaying oscillations are measured. As we shall see, use of the device in plucked mode gives rise to a fractional differential equation.

2. Device modelling

For modelling purposes, we assume that the spider is set into motion in a homogeneous incompressible fluid that has a constant viscosity. Though it would be of significant practical value to the oil well logging industry to produce a viscometer

that was able to measure some of the properties of non-Newtonian fluids (and the spider is clearly capable of doing this), for simplicity we will restrict the analysis in this study to linear viscous fluids. The fluid flow is governed by the Navier–Stokes equations

$$\mathbf{q}_t + (\mathbf{q}.\nabla)\mathbf{q} = -\frac{1}{\rho}\nabla p + \nu\nabla^2\mathbf{q} \tag{1}$$

$$\nabla.\mathbf{q} = 0 \tag{2}$$

where $\mathbf{q}$ denotes the fluid velocity, p denotes pressure, t denotes time and ρ and ν are the fluid density and kinematic viscosity, respectively. Eqs. (1) and (2) must be solved for all regions where fluid is present, subject to the standard no slip condition which is imposed on all rigid boundaries. Clearly, one possible approach would be to solve these equations numerically, including full details of all the geometry of the device. Below, we give details of an alternative approach, where a one-dimensional model is proposed to analyse the behaviour of the device.

2.1. Sensor motion: Leg behaviour

During motion, strain is produced in inter-connecting parts of the viscometer. The most significant such strains are those involving the legs connecting the plate to the main viscometer body. For simplicity, we assume henceforth that all motion of the device occurs only as a result of the deformation of these legs. For each of the legs, the elastic restoring force F_{er} may be written

$$F_{er} \equiv \frac{s^3 EdA}{\ell^3},$$

where s, ℓ and d, respectively, denote leg width, leg length and leg depth (which, in the specific device under consideration in this study, is also equal to the plate depth), E is the Young's modulus of the leg material, and A is the amplitude of motion. If we further assume that the undamped device frequency ω_0 (for a device with N legs) depends on the total mass $M_p = aBd\rho_s$ of the plate, then

$$\omega_0 = \sqrt{\frac{NF_{er}}{AM_p}} = \sqrt{\frac{NEs^3}{l^3 aB\rho_s}}$$

where a is the length of the plate, B is the plate width, and ρ_s is the density of the plate material.

3. The forced spider

For reasons that will become apparent, the main focus of this study will be an analysis of the spider in plucked mode. For completeness, however, it is worth briefly summarising the results for cases when the device is used in forced mode. We assume that coordinates are defined so that the plate lies in the (x, z)-plane and that the device can move only in this plane, and proceed as though the plate were infinite in extent in both the x and z directions (an assumption that can be later verified to be justified so long as the viscous penetration depth is much smaller than the plate length and width) and has zero thickness. If the oscillations are forced then $\boldsymbol{q} = (U_0\mathrm{Re}(\exp(-\mathrm{i}\omega t)), 0, 0)$ at $y = 0$, where U_0 is the amplitude of the motion and ω the frequency. If we now assume that $\boldsymbol{q}$ is non-zero only in its first component, which is of the form $u(y, t)$, then it is easy to show that the motion above the plate is governed by the equation

$$u_t = \nu u_{yy}$$

where $t \geq 0$, $y \in [0, \infty)$, $x \in (-\infty, \infty)$, $z \in (-\infty, \infty)$ and $u(0, t) = U_0 \cos\omega t$. The solution is given by

$$u = U_0 \mathrm{e}^{-y/\delta}\mathrm{Re}(\mathrm{e}^{\mathrm{i}(y/\delta-\omega t)}) = U_0 \mathrm{e}^{-y/\delta}\cos(y/\delta - \omega t)$$

where $\delta = \sqrt{2\nu/\omega}$ is the so-called "viscous penetration depth". The frictional force S in the x-direction on the plate (whose surface area top and bottom is given by $2Ba$) is given by

$$S = 2aB\mu u_y|_{y=0} = -2aB\sqrt{\omega\mu\rho}U_0\cos(\omega t + \pi/4)$$

and the average power P over a period of oscillation is thus

$$P|_{y=0} = \frac{\omega}{2\pi}\left|\int_0^{2\pi/\omega} Su|_{y=0}\,\mathrm{d}t\right| = \sqrt{\frac{\omega\mu\rho}{2}}aBU_0^2.$$

We therefore find that the fluid viscosity μ is given by

$$\mu = \frac{2}{\omega\rho}\left(\frac{P|_{y=0}}{aBU_0^2}\right)^2$$

and, in principle, the viscosity may be determined by measuring the power and amplitude of the motion. Though this appears to be an attractive strategy for viscometry, it involves some practical difficulties. First, it is frequently rather hard to monitor both the power supplied to the device and the amplitude of the motion. More seriously, experiments that have been carried out have shown that, when the spider is operated in this mode, the legs can lose their structural integrity and the device may break.

Although these difficulties mean that, for practical purposes, the spider is likely to prove a more successful instrument when used in plucked mode (as described below), it may still be the case that progress in the forced mode may be possible at a later date. An advantage of forced mode is that the device may be used not only with a top plate added, but is also well suited to measuring the key properties of viscoelastic fluids. For the present however, we do not consider the forced spider further, referring the reader instead to [8] (where the viscoelastic case is also considered) for details.

4. The "plucked spider"

We now consider the operation of the MEMS viscometer in "plucked" mode, where the device is subjected to a known initial displacement X, held stationary at the displaced position, and then released. The subsequent decaying oscillations are then measured electronically using the circuitry in the plate. In contrast to the analysis carried out in Section 3, the displacement of the plate is now unknown. The task of the modelling that will be carried out below is therefore to predict the decaying oscillations of the plate and hence infer the viscosity of the surrounding fluid.

We assume that the displacement x of the plate may be described by a simple spring model, as discussed in Section 2.1. The plate is retarded by both the elastic damping r (dimensions kg/s) provided by the legs and the viscous shear stress exerted on the plate by the surrounding fluid. The displacement of the plate therefore satisfies the equation of motion

$$\rho_s dBa\ddot{x} + r\dot{x} + k^2 x = 2Ba\mu u_y\,|_{y=0}\,.$$

Here $k^2 = \omega_0^2 \rho_s dBa$, a dot denotes differentiation with respect to time, and the boundary conditions are $x(0) = X$, $\dot{x}(0) = 0$.

To convert the plucked spider problem to a fractional differential equation, we first solve the problem in the fluid. This is given once again by

$$u_t = \nu u_{yy}$$

with $u(0, t) = \dot{x}(t)$, $u(y, 0) = 0$ and $u \to 0$ as $y \to \infty$. This is most easily done by using a Laplace transform. Assuming that $\dot{x}$ is suitably well-behaved (if it is not then the device will be useless as a viscometer), we find that

$$u(y, t) = \int_0^t \frac{y\dot{x}(s)\exp\left(-\frac{y^2}{4\nu(t-s)}\right)}{2\sqrt{\pi\nu}(t-s)^{3/2}}\,\mathrm{d}s$$

and so the quantity u_y is given by

$$u_y(y, t) = \int_0^t \frac{\dot{x}(s)\exp\left(-\frac{y^2}{4\nu(t-s)}\right)}{\sqrt{4\pi\nu}(t-s)^{3/2}}\left[1 - \frac{y^2}{2\nu(t-s)}\right]\mathrm{d}s.$$

To determine the limit of u_y as $y \to 0$, it is convenient to integrate by parts, giving

$$u_y(y, t) = -\frac{1}{4\nu\sqrt{\pi\nu}}\left[\left[-\dot{x}(s)\frac{4\nu\exp\left(-\frac{y^2}{4\nu(t-s)}\right)}{\sqrt{t-s}}\right]_0^t + \int_0^t \ddot{x}(s)\frac{4\nu\exp\left(-\frac{y^2}{4\nu(t-s)}\right)}{\sqrt{t-s}}\,\mathrm{d}s\right],$$

so that

$$\lim_{y\to 0} u_y(y, t) = -\frac{1}{\sqrt{\pi\nu}}\int_0^t \frac{\ddot{x}(s)}{\sqrt{t-s}}\,\mathrm{d}s.$$

The equation of motion of the plucked spider is therefore given by

$$\rho_s dBa\ddot{x} + r\dot{x} + k^2 x = -\frac{2Ba\mu}{\sqrt{\pi\nu}}\int_0^t \frac{\ddot{x}(s)}{\sqrt{t-s}}\,\mathrm{d}s. \tag{3}$$

To express (3) as a fractional differential equation, we use the Caputo definition of a fractional derivative (see, for example [6]) wherein we define the μth Caputo fractional derivative $(D_*^\mu f)(t)$ of the function $f(t)$ by

$$(D_*^\mu f)(t) = (J^{m-\mu} f^{(m)})(t) = \frac{1}{\Gamma(m-\mu)}\int_0^t (t-s)^{m-\mu-1} f^{(m)}(s)\,\mathrm{d}s \tag{4}$$

where $m-1 < \mu \le m$, m is a natural number and $t > 0$. The Caputo definition of the fractional derivative enjoys a significant advantage over the alternative (Riemann–Liouville) definition of the fractional derivative, for it allows the initial conditions for the problem to be specified in a natural manner. In contrast, the Riemann–Liouville definition (see, for example [6])

requires conditions to be specified in terms of fractional derivatives or integrals, a form in which they are not normally known.

It is also convenient to non-dimensionalise (3) by setting $x = X\tilde{x}$ and $t = (\sqrt{\rho_s Bda}/k)\tilde{t}$. Dropping the tildes here and henceforth for simplicity and using (4), we find that (3) may be written

$$D_*^2 x + \beta\sqrt{\pi} D_*^{3/2} x + \alpha D_*^1 x + x = 0 \quad (x(0) = 1, D_*^1 x(0) = 0) \tag{5}$$

where $\alpha = r/(k\sqrt{\rho_s Bda})$ and $\beta = (4\mu\rho/k\pi)^{1/2}(Ba/\rho_s^3 d^3)^{1/4}$. We note that (5) is closely related to the Bagley–Torvik equation described in [1], and also that solutions to the problem depend only on the two non-dimensional combinations α and β of the problem parameters.

4.1. Asymptotic behaviour of the solution

For both theoretical and practical purposes it is useful to determine the asymptotic behaviour of the solution to (5) for $t \ll 1$ and as $t \to \infty$. This may be done in a number of ways, though the simplest is probably to take a Laplace transform of the coupled problem (see [8] for details). The (non-dimensional) result is that

$$x(t) \sim 1 - \frac{t^2}{2} + O(t^{5/2}) \quad (t \to 0+), \qquad x(t) \sim \frac{\beta\pi}{t^{3/2}} + O(t^{-5/2}) \quad (t \to \infty). \tag{6}$$

From a practical point of view, the behaviour as $t \to \infty$ is significant, for in most viscometers that employ some sort of "plucking" mechanism, it is routinely assumed that the motion of the device decays exponentially. This guides both the choice of sensor that is normally used to measure the motion and the *modus operandi* of the data-fitting process used to finally infer the fluid viscosity from measurements of the decay. We conclude that, for the current device, allowances will have to be made for the fact that the motion decays algebraically rather than exponentially.

4.2. Solution of the governing equation

We now focus on (5) with $\alpha = 0$. Choosing to ignore the leg damping is tantamount to assuming that the device is retarded mainly by the viscous damping of the surrounding fluid. If this is not the case and the leg damping becomes important, then it is clear on physical grounds that the usefulness and accuracy of the device as a viscometer will be seriously compromised. We set $y = x - 1$ and note that (5) now becomes

$$D_*^2 y + \beta\sqrt{\pi} D_*^{3/2} y + y = -1 \qquad (D_*^1 y(0) = 0, \quad y(0) = 0).$$

The solution to this fractional differential equation is given by (see, for example [7])

$$y(t) = \int_0^t G(t-u)(-1)\mathrm{d}u$$

where

$$G(t) = \sum_{k=0}^{\infty} \frac{(-1)^k}{k!} t^{2k+1} E^{(k)}_{\frac{1}{2}, 2+\frac{3k}{2}}(-\beta\sqrt{\pi}\sqrt{t})$$

and $E^{(k)}_{\lambda,\mu}$ is the kth derivative of the generalised Mittag–Leffler function, given by

$$E^{(k)}_{\lambda,\mu}(t) = \sum_{j=0}^{\infty} \frac{(j+k)! t^j}{j!\Gamma(\lambda j + \lambda k + \mu)}. \tag{7}$$

(Note that, since for large j it is true that $\Gamma(j) \sim \sqrt{2\pi}\mathrm{e}^{-j} j^{j-1/2}$, it may easily be shown by using the ratio test that (7) converges for all finite t.)

The solution to (5) with $\alpha = 0$ is therefore given by

$$x(t) = 1 - \int_0^t G(t-u)\,\mathrm{d}u.$$

Assuming that term-by-term integration is possible (though this does not seem easy to show), we find that

$$x(t) = 1 - \sum_{j=0}^{\infty}\sum_{k=0}^{\infty} \frac{(-1)^k(-\beta\sqrt{\pi})^j (j+k)! t^{2+2k+\frac{j}{2}}}{j!k!(2+2k+\frac{j}{2})\Gamma(2+2k+\frac{j}{2})}. \tag{8}$$

As $\beta \to 0$, we may verify that, as expected, the solution reduces to

$$x \to 1 - \sum_{k=0}^{\infty} \frac{(-1)^k t^{2+2k}}{(2+2k)!} = \cos(t).$$

It is also convenient to note that, since

$$\sum_{k=0}^{\infty}\frac{(-1)^k(-\beta\sqrt{\pi})^j(j+k)!t^{2+2k+\frac{j}{2}}}{j!k!(2+2k+\frac{j}{2})\Gamma(2+2k+\frac{j}{2})}=\frac{2(-\beta\sqrt{\pi})^jt^{2+\frac{j}{2}}}{(4+j)\Gamma(2+\frac{j}{2})}\,{}_1F_2\left([j+1],\left[\frac{j+8}{4},\frac{j+6}{4}\right],-\frac{t^2}{4}\right)$$

the solution may be conveniently expressed in terms of the extended hypergeometric function as

$$x(t)=1-\sum_{j=0}^{\infty}\frac{2(-\beta\sqrt{\pi})^jt^{2+\frac{j}{2}}}{(4+j)\Gamma(2+\frac{j}{2})}\,{}_1F_2\left([j+1],\left[\frac{j+8}{4},\frac{j+6}{4}\right],-\frac{t^2}{4}\right). \tag{9}$$

Fractional differential equation solutions such as (9) have been presented in many previous studies; in this case, however, we aim to try to use the solution to provide practical information that may be used for device optimisation. We shall presently address the numerical solution of (5), however, we note for the present that the closed form solution (9) is only of any practical use if it converges for a large range of the parameters involved. A standard asymptotic expansion may be used to show that, as $t\to 0+$,

$${}_1F_2\left([j+1],\left[\frac{j+8}{4},\frac{j+6}{4}\right],-\frac{t^2}{4}\right)\sim 1-\frac{4(j+1)}{(j+6)(j+8)}t^2+O(t^4)$$

and the ratio test may then be used to show that the series converges. When t and β are both relatively small, either (8) or (9) may be used in suitably truncated form to evaluate the solution numerically in an efficient and accurate manner. Unfortunately when β and t are not small the leading terms of both of the above series become large, much cancellation occurs, and numerical evaluation becomes a very difficult matter. Though numerical experiments might lead one to conclude that the radii of convergence of both (8) and (9) are finite, it may be shown that both series are in fact convergent for all finite positive values of β and t by noting that, if we set

$$S(\beta,t)=\sum_{j=0}^{\infty}\sum_{k=0}^{\infty}\frac{(-1)^k(-\beta\sqrt{\pi})^j(j+k)!t^{2+2k+j/2}}{j!k!\Gamma(3+2k+j/2)}$$

then

$$\begin{aligned}S(\beta,t)&=\sum_{n=0}^{\infty}\sum_{j=0}^{n}\frac{(-1)^n n!(\beta\sqrt{\pi})^jt^{2+2n-3j/2}}{j!(n-j)!\Gamma(3+2n-3j/2)}\\&=\sum_{n=0}^{\infty}(-1)^nt^{2+2n}\sum_{j=0}^{n}\binom{n}{j}\frac{(\beta\sqrt{\pi}t^{-3/2})^j}{\Gamma(3+2n-3j/2)}.\end{aligned}$$

If we now express the reciprocal Gamma function using Hankel's contour integral expression (see, for example [9]), then we may write

$$\begin{aligned}S(\beta,t)&=\sum_{n=0}^{\infty}(-1)^nt^{2+2n}\frac{1}{2\pi\mathrm{i}}\int_{-\infty}^{0+}\mathrm{e}^ss^{-3-2n}\sum_{j=0}^{n}\binom{n}{j}(\beta\sqrt{\pi}(st^{-1})^{3/2})^j\,\mathrm{d}s\\&=\sum_{n=0}^{\infty}(-1)^nt^{2+2n}\frac{1}{2\pi\mathrm{i}}\int_{-\infty}^{0+}\mathrm{e}^ss^{-3-2n}(1+\beta\sqrt{\pi}(st^{-1})^{3/2})^n\,\mathrm{d}s.\end{aligned}$$

Setting $s=z^2t$ and summing the series now shows that

$$S(\beta,t)=\frac{1}{\pi\mathrm{i}}\int_{c-\mathrm{i}\infty}^{c+\mathrm{i}\infty}\frac{\mathrm{e}^{tz^2}}{z(z^4+\beta\sqrt{\pi}z^3+1)}\mathrm{d}z \tag{10}$$

where c is chosen so that all poles of the integrand in (10) lie to the left of the integration contour. The integral (10) may now be evaluated numerically with ease for arbitrary positive values of β and t so that the exact solution may be used for comparison purposes.

Finally, we note that even if $\alpha\neq 0$, it is still possible to express the solution to (5) in closed form (see, for example [5]). Unfortunately, the solution thus obtained is of a rather involved nature and is inconvenient to use for practical purposes.

4.3. Numerical solution of the governing equation

A successful numerical strategy for the solution of (5) was discussed in full in [8]. We let x_i denote the approximate value of $x(t)$ at time $t=t_i$ with $i=0,1,\ldots,N$ and $t_0=0$ and, for simplicity, use a constant time step δt so that $t_{i+1}-t_i=\delta t$. The initial conditions are that the plate starts from a stationary position at a (dimensional) distance X from the origin, so that $\dot{x}(0)=0, x(0)=1$. Central differences are used to approximate the first and second derivatives of x with respect to t, and the fractional term in the equation is dealt with by approximating the integral in the Caputo definition of the fractional

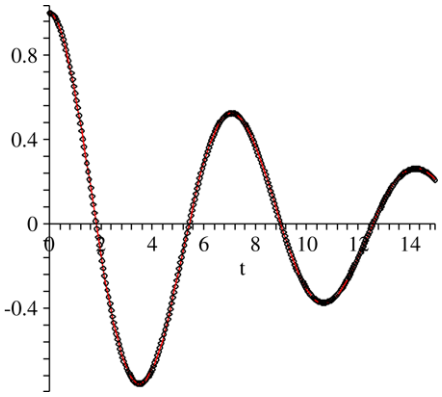

Fig. 2. Comparison between numerical solution (symbols) and exact solution (solid line), for parameters $\alpha = 0$, $\beta = 1/5$, $\delta t = 0.05$.

derivative in the simplest possible fashion at time t_i, namely by assuming that $\ddot{x}$ is linear on each interval $[t_j, t_{j+1}]$ and using the trapezium rule. Eq. (5) may then be approximated using

$$\frac{x_{i+1} - 2x_i + x_{i-1}}{\delta t^2} + \alpha\left(\frac{x_{i+1} - x_{i-1}}{2\delta t}\right) + x_i + \beta\left(\frac{x_{i+1} - x_i - x_{i-1} + x_{i-2}}{\delta t^{\frac{3}{2}}}\right)$$
$$= -\beta\sum_{j=1}^{i-1}\frac{x_{j+1} - x_j - x_{j-1} + x_{j-2}}{\delta t^{\frac{3}{2}}}(\sqrt{i-j+1} - \sqrt{i-j}). \tag{11}$$

This general scheme (11) may now be rearranged to give x_{i+1} in terms of x_i, x_{i-1}, and x_{i-2}, allowing all the x_i to be determined for $i \geq 3$. We introduce an artificial mesh point for $i = -1$ and determine x_0, x_1, and x_2 independently. We use the boundary condition $x(0) = 1$ to set $x_0 = 1$ and introduce a central difference to show that $x_{-1} = x_1$. The asymptotic solution (6) for $t \ll 1$ is used to determine x_1. Since the integral term in Eq. (5) is zero when $t = 0$, the scheme given by (11) may now be applied with $i = 1$ and all terms involving β are set equal to zero to yield the value of x_2 so that the calculation may begin. The final (dimensionless) numerical scheme is thus

$$x_0 = 1, \qquad x_{-1} = x_1, \qquad x_1 = 1 - \frac{\delta t^2}{2}$$
$$x_2 = \left(\frac{2}{2+\alpha\delta t}\right)\left[x_1(2-\delta t^2) + x_0\left(\frac{\alpha\delta t}{2} - 1\right)\right]$$
$$x_{i+1} = \left(\frac{2}{2+\alpha\delta t + 2\beta\delta t^{1/2}}\right)\left[x_i(2-\delta t^2+\beta\delta t^{1/2}) + x_{i-1}\left(\frac{\alpha\delta t}{2} + \beta\delta t^{1/2} - 1\right)\right.$$
$$\left. - x_{i-2}\beta\delta t^{1/2} - \beta\sum_{j=1}^{i-1}\left(\frac{x_{j+1} - x_j - x_{j-1} + x_{j-2}}{\delta t^{\frac{3}{2}}}\right)(\sqrt{i-j+1} - \sqrt{i-j})\right]. \tag{12}$$

All of the usual numerical tests may be carried out to verify that the proposed scheme is consistent and convergent; we suppress the results of these tests for brevity. Though the scheme is relatively quick to run, the fractional derivative term increases the execution time greatly in comparison to similar methods for standard differential equations, as is familiarly encountered for such equations. Convergence analysis may also be carried out in a standard fashion if required. It should also be noted that many alternative numerical methods may be proposed for the solution of (5), and many such methods have also been analysed for consistency, convergence and economy. For further details the reader is referred to [4].

The exact solution is convenient for comparison purposes. Fig. 2 shows a typical case; we observe good agreement between the numerical and exact solutions (parameters used: $\alpha = 0$, $\beta = 1/5$, $\delta t = 0.05$).

4.4. A theoretical approach to device design

Having carried out a substantial amount of both theoretical and numerical analysis of the "spider", we are now in a position to help to optimise the design of the device using what we have learned. In particular, we would like to know for what kinds of fluid a MEMS viscometer of a given size might be expected to give practically useable results.

First, let us consider the time scale of the device. We previously set $t = T\bar{t}$ where $T = \sqrt{\rho_s Bda}/k$. For the device shown in Fig. 1, we have $\rho_s \simeq 2320$ kg m^{-3}, $B \simeq 1.6$ mm, $d \simeq 20$ μm and $a \simeq 2.4$ mm so that the weight $W = \rho_s Bda$ of the device is given by $W \simeq 1.78 \times 10^{-7}$ kg. There are two ways of determining the constant k for practical comparisons. One way is to infer k from a series of *in vacuo* experiments. When we did this it was found that $k \sim 95$ kg$^{1/2}$/s (a value that will

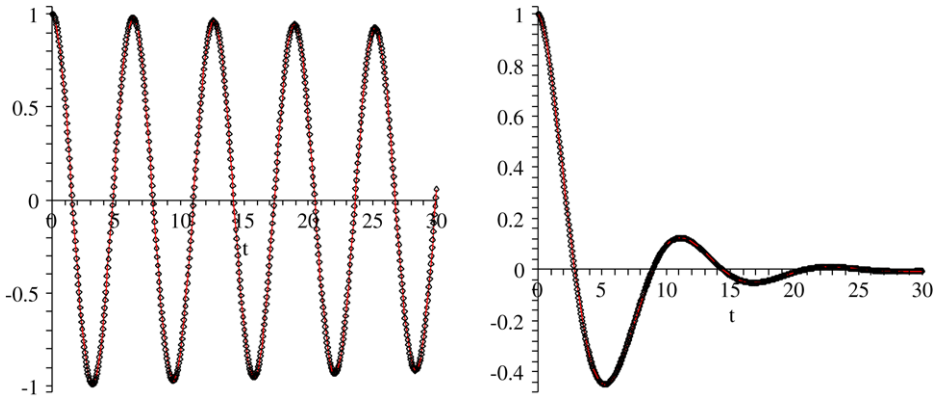

Fig. 3. Numerical solution (symbols) and exact solution calculated from (10) (solid line) for two cases with $\alpha = 0$ and $\delta t = 0.05$ (left hand diagram: $\beta = 0.005$; right hand diagram: $\beta = 1$).

henceforth be used in our results and comparisons). Alternatively, one might simply calculate k using the relationship given earlier which amounts to

$$k^2 = \omega_0^2 \rho_s dBa = \frac{NEs^3 d}{\ell^3}. \tag{13}$$

Using $N = 48$ (24 legs per side), $E = 125.8$ GPa [3], $s = 4 \times 10^{-5}$ and $\ell = 5 \times 10^{-4}$ gives $k \sim 247$ kg$^{1/2}$/s. Though this value is larger than that determined by experiment by a factor of roughly 2.5, the mere fact that the calculation gives a value that is the same order of magnitude as the experimental result is encouraging when one considers the number of approximations that are present in (13).

Using $W \simeq 1.78 \times 10^{-7}$ kg and $k \simeq 95$ kg$^{1/2}$/s as explained above, yields a timescale of $T \simeq 4.4 \times 10^{-6}$ s, from which we immediately conclude that any motion sensors that are used will have to be capable of measuring over microsecond time scales. If the leg damping is ignored (as stated earlier, if this is not justified then it is unlikely that the device will ever be useful) then the only other non-dimensional parameter of importance is $\beta = (4\mu\rho/k\pi)^{1/2}(Ba/\rho_s^3 d^3)^{1/4}$. Fig. 3 shows numerical solutions with $\alpha = 0$ for what we might regard as two extreme situations, namely the values $\beta = 0.005$ (where the oscillations decrease so slowly in magnitude that the decay would be hard to measure) and $\beta = 1$ (where the decay is so rapid that not enough data would be collected). From these results we conclude that, for the device to have any chance of functioning correctly, we require

$$0.005 < \left(\frac{4\mu\rho}{k\pi}\right)^{1/2} \left(\frac{Ba}{\rho_s^3 d^3}\right)^{1/4} < 1.$$

Using values $k \sim 95$ kg$^{1/2}$/s, $B = 1.6$ mm, $\rho_s = 2320$ kg m^{-3}, $a = 2.4$ mm, $d = 20$ μm, we find that the imposed limits on β amount to $0.01 < \mu\rho < 381$ kg^2 m^{-4} s^{-1}. The device will therefore be useful for fluids such as water (where at ambient temperatures $\mu\rho \sim 1$) and a range of other fluids that are commonly encountered downhole. Finally, we note that the key non-dimensional parameter β contains all of the information that we need to determine how the device specifications and material properties would have to change if the properties of a substantially different type of fluid were to be measured.

4.5. A nonlinear fractional differential equation

The assumption that the legs of the MEMS device that has been analysed give rise to behaviour that mimics a linear spring is unlikely to be exactly true in practice. It is well known that, for most springs, a more accurate representation of the elastic force F is given by $F = -k^2 x + \phi x^3$ where $\phi < 0$ is identified with a so-called "hard" spring and $\phi > 0$ with a "soft" spring. We therefore now extend our analysis to include the case of such springs, where the (non-dimensional) governing equation is

$$D_*^2 x + \beta\sqrt{\pi} D_*^{3/2} x + \alpha D_*^1 x + x + \epsilon x^3 = 0 \quad (x(0) = 1, D_*^1 x(0) = 0) \tag{14}$$

and the dimensionless parameter ϵ is greater than (less than) zero for a hard (soft) spring. It is well known that in the case $\alpha = \beta = 0, \epsilon > 0$, all solutions of (14) are bounded, oscillatory and periodic, and it therefore seems likely that for non-zero values of α and/or β, the nonlinear spring term will simply introduce an extra retardation term.

Though there appears to be little hope of finding any closed-form solutions to (14), the numerical scheme developed in Section 4.3 enjoys the great advantage that it may easily be modified to include the nonlinear term. The only changes that need to be made involve setting $x_1 = x_{-1} = 1 - (1 + \epsilon)\delta t^2/2$ and replacing the term $x_1(2 - \delta t^2)$ by $x_1(2 - \delta t^2 - \epsilon x_1^2 \delta t^2)$ in the definition for x_2 and the term $x_i(2 - \delta t^2 + \beta\delta t^{1/2})$ by $x_i(2 - \delta t^2 + \beta\delta t^{1/2} - \epsilon x_i^2 \delta t^2)$ in the definition for x_i in (12).

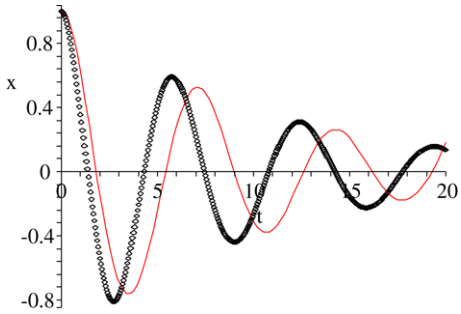

Fig. 4. Comparison between numerical solution (symbols) for nonlinear case with $\epsilon = 1$ and exact solution (solid line, $\epsilon = 0$), for parameters $\alpha = 0$, $\beta = 1/5$, $\delta t = 0.05$.

Fig. 4 compares the numerical solution to the nonlinear problem (with $\epsilon = 1$: symbols) and the exact solution ($\epsilon = 0$: solid line) for parameter values $\alpha = 0$, $\beta = 1/5$ and $\delta t = 0.05$. We note that the nonlinear solution has a slightly greater amplitude and also exhibits a phase difference. We carried out many other numerical experiments and the results shown in Fig. 4 are typical, confirming that though a difference in both phase and amplitude are to be expected, the generic behaviour of the device remains unchanged.

5. Further results and conclusions

The operation of a novel MEMS viscometer has been analysed using a combination of theory and numerical calculations. It has been shown that, using the model predictions, device dimensions and other properties can be specified that will allow the device to function efficiently for fluids with a given viscosity and density range. The analysis also showed that, unlike many similar devices, the decay of the motion of the moving component of the viscometer is algebraic rather than exponential — a matter that is likely to be of practical significance for device designers and manufacturers.

As mentioned above, it is ultimately desirable to use the device to determine some of the properties of non-Newtonian fluids. As we have seen, device optimisation is probably only really possible if a complete theory of the device is available, and though the current theory could be extended to encompass viscoelastic effects, it is not easy to see what could be done for nonlinear (for example, pseudoplastic) fluids.

If the legs of the device are modelled as nonlinear (Duffing-type) springs, then it has been shown that, though no exact solution is available, the problem may be solved numerically with ease. As usual with more complicated models, a key challenge if the nonlinear spring assumption is used will be to determine the constants that appear in the model with accuracy. In general, a full experimental programme is required if the device is to be transformed from being an interesting idea to a working commercial device.

Finally, we note that, assessed in comparison to viscometers in general, the accuracy of the device is not exceptional; crucially, however, the device is sufficiently accurate in hostile conditions and sufficiently small to be deployed downhole. It is important to realise that, for efficient and cost-effective oil exploration, a trade-off will almost certainly have to be made between measurement precision and the ability to perform in challenging surroundings and operate in a wide range of fluids.

Acknowledgements

The authors are grateful to Chris Howls and Colin Please (University of Southampton) for discussions and also to Adri Olde Daalhuis (University of Edinburgh) for his suggestions regarding the convergence properties of the solution.

References

[1] R.L. Bagley, P.J. Torvik, On the appearance of the fractional derivative in the behavior of real materials, J. Appl. Mech. 51 (1984) 294–298.
[2] A.R.H. Goodwin, E.P. Donzier, O. Vancauwenberghe, A.D. Fitt, K.A. Ronaldson, W.A. Wakeham, M.M. de Lara, F. Marty, B. Mercier, A vibrating edge supported plate, fabricated by the methods of micro electro mechanical system for the simultaneous measurement of density and viscosity: Results for methylbenzene and octane at temperatures between (323 and 423) K and pressures in the range (0.1–68) MPa, J. Chem. Eng. Data 51 (2006) 190–208.
[3] A.R.H. Goodwin, A.D. Fitt, K.A. Ronaldson, W.A. Wakeham, A vibrating plate fabricated by the methods of microelectromechanical systems (MEMS) for the simultaneous measurement of density and viscosity: Results for argon at temperatures between 323 and 423 K at pressures up to 68 MPa, Int. J. Thermophys. 27 (2006) 1650–1676.
[4] A.A. Kilbas, H.M. Srivastava, J.J. Trujillo, Theory and Applications of Fractional Differential Equations, Elsevier Science, 2006, pp. 272–277.
[5] Y.F. Luchko, H.M. Srivastava, The exact solution of certain differential equations of fractional order by using operational calculus, Comput. Math. Appl. 29 (1995) 73–85.
[6] F. Mainardi, R. Gorenflo, On Mittag–Leffler-type functions in fractional evolution processes, J. Comp. Appl. Math. 118 (2000) 283–299.
[7] I. Podlubny, Fractional Differential Equations, Academic Press, San Diego, 1999.
[8] K.A. Ronaldson, A.D. Fitt, A.R.H. Goodwin, W.A. Wakeham, Transversely oscillating MEMS viscometer: The “Spider”, Int. J. Thermophys. 27 (2006) 1677–1695.
[9] E.T. Whittaker, G.N. Watson, Modern Analysis, fourth edition, Cambridge University Press, 1940 (Chapter 12).